Journal of The Electrochemical Society, **156** (1) J16-J19 (2009)
0013-4651/2008/156(1)/J16/4/$23.00 © The Electrochemical Society

Fabrication and CO Sensing Properties of Mesostructured ZnO Gas Sensors

Chueh-Yang Liu,[a,z] Chia-Fu Chen,[b] and Jih-Perng Leu[a]

[a]*Department of Materials Science and Engineering, National Chiao-Tung University, Hsinchu 300, Taiwan*
[b]*Institutes of Material and System Engineering, MingDao University, ChangHua 52345, Taiwan*

This study presents the synthesis of mesostructured ZnO using a template replication method and the fabrication of a carbon monoxide sensor using the synthesized ZnO using the dielectrophoresis process. The mesoporous carbon, CMK-3, was employed for the template and zinc nitrite was used as the precursor for synthesizing the ordered porous ZnO. The mesostructured ZnO was analyzed using X-ray diffraction (XRD) patterns, scanning electron microscopy, transmission electron microscopy, selected area electron diffraction, and N_2 adsorption–desorption isotherms. The XRD patterns indicated that the ZnO exhibited a highly ordered structure after the template was removed. The morphology of the ZnO was randomly oriented and the structure was polycrystalline. The surface area, pore volume, and pore size of the porous ZnO were 61.3 $m^2\ g^{-1}$, 0.31 $cm^3\ g^{-1}$, and 5.3 nm, respectively. When CO gas was injected, the optimum sensitivities at 250°C were 12.1, 14.6, 18.4, 26.0, and 60% when the CO concentrations were 10, 20, 30, 50, and 70 ppm, respectively.
 [DOI: 10.1149/1.3021044]

Manuscript submitted September 2, 2008; revised manuscript received October 10, 2008. Published November 14, 2008.

Carbon monoxide (CO) is the main product from incomplete combustion processes and is toxic even at concentrations lower than 100 ppm. Its toxicity is dangerously magnified by the fact that it is colorless and odorless, and thus very difficult to detect. There has been extensive research into developing solid-state CO sensors using semiconductor oxides, solid electrolytes, and organic semiconductors.[1] Conventional solid-state sensors have been fabricated by adding noble metal elements such as Pt, Au, and Pt into the oxide semiconductors such as SnO_2, Fe_2O_3, and ZnO.[2] However, few of them perform satisfactorily in terms of sensitivity and selectivity in the detection of CO.

Recently, the semiconductive metal oxide gas sensors have been developed. The sensors have low cost, high sensitivity, fast response, and are compatible with silicon materials. ZnO is an interesting n-type semiconductor with a large bandgap energy of 3.4 eV at room temperature, large excitonic energy, low electron affinity, and high mechanical strength.[3] ZnO is an intriguing possibility as a sensory material due to the high mobility of its conductive electrons and its good chemical and thermal stability. Several techniques have been used to prepare ZnO sensors, including chemical vapor deposition, the sol-gel process, and evaporation.[4-6] A new method for synthesizing semiconductor metal oxide sensors was recently developed by Wagner et al. The semiconductor porous metal oxides not only have large surface areas and uniform pore dimensions, but also show a superior sensory performance to nonporous samples of the same metal oxides.[7]

A good example of a solid template for porous metal oxides is mesoporous silica. In the procedure, a matrix structure is impregnated with the precursor and transformed into the porous oxide. Using mesoporous silicas for the matrix, several metal oxides have been yielded, including Co_3O_4, CrO_2, and Fe_3O_4.[8-10] Tian et al. synthesized several porous metal oxides using microwave-digested mesoporous silica.[11] They reported that these mesoporous metal oxides exhibit original and highly ordered structures as well as large surface areas. They also synthesized mesoporous and mesorelief oxides with gyroidal structures.[12] The metal oxide crystal showed double-scale ordering, and a single-crystalline structure could be observed. However, while several porous metal oxides can be synthesized using mesoporous silica as a template, mesoporous ZnO cannot because the removal of the silica templates HF or concentrated sodium hydroxide (NaOH) solutions. Mesoporous ZnO is unsuited for this as it is soluble both when the pH is very low and very high. Therefore, mesoporous carbon is used instead of the mesoporous silica as the solid template for synthesizing mesoporous ZnO. The mesoporous carbon is first prepared through a structure replication procedure, and then a mesoporous metal oxide is infused into the replica. This process has been shown to be successful in the preparation of mesoporous SiO_2, CeO_2, and TiO_2.[13-15] Until now, porous ZnO materials for gas sensors were prepared using conventional sol-gel technology.[16] This paper presents the synthesis of ordered mesoporous ZnO by use of mesoporous carbon as the structure matrix and the fabrication of a mesostructured porous ZnO sensory device through dielectrophoresis (DEP) manipulation.

Experimental

Mesoporous SBA-15 silica was synthesized through modification of a known procedure in the literature of the field.[17] An 8.5 g P-123 block copolymer (Sigma) was mixed with 325 mL HCl (1.6 mol L^{-1}) and stirred for 24 h at 308 K. After the addition of 18.7 g tetraethyl orthosilicate (Merck) the mixture was stirred at 308 K for another 24 h. The resulting gel was transferred to a Teflon-lined autoclave and kept at 413 K for 24 h. The solid product was filtered off, washed with water, and calcined at 823 K for 6 h (heating rate 2 K min^{-1}). CMK-3 carbon was prepared according to another procedure in the literature[18] by impregnating SBA-15 with sucrose as the carbon source, which was converted to carbon by pyrolysis in a vacuum at 1173 K. The silica matrix was removed by stirring the silica/carbon sample in a 5% HF solution for 4 h at room temperature. Mesoporous ZnO was prepared by immersing 0.5 g CMK-3 carbon in 20 mL of a solution made up of $Zn(NO_3)_2$ in tetrahydrofuran (1.5 mol L^{-1}) and stirring at room temperature for 6 h. After filtration the impregnated carbon was dried at ambient temperature, heated in an air atmosphere to 573 K at a constant rate of 2.5 K min^{-1}, and kept at that temperature for 2 h to convert zinc nitrate to zinc oxide. This procedure was repeated twice. The resultant product was a powder without any specific particle morphology.

X-ray diffraction (XRD) patterns were obtained using a Bede/D1 diffractometer with Cu Kα radiation (1.543 Å) at a voltage of 40 kV and current of 40 mA. Scanning electron microscopy (SEM) was performed using a JEOL 6700F electron microscope at an acceleration voltage of 3 kV. The mesoporous carbon was adhered to the carbon tape and sputtered with gold to the image. The nitrogen adsorption–desorption isotherms were measured at −196°C using a NOVA 1000e system in static measurement mode. The samples were degassed at 150°C for 3 h before measurement. The specific surface areas were determined by the Brunauer–Emmett–Teller method based on the adsorption branches. The pore diameter and pore size distribution were measured from the desorption branches obtained by the Barrett–Joyner–Halenda (BJH) method. Transmission electron microscopy (TEM) and selected area electron diffraction (SAED) were used to clarify the structure of mesoporous ZnO

[z] E-mail: Jason.liu1107@msa.hinet.net

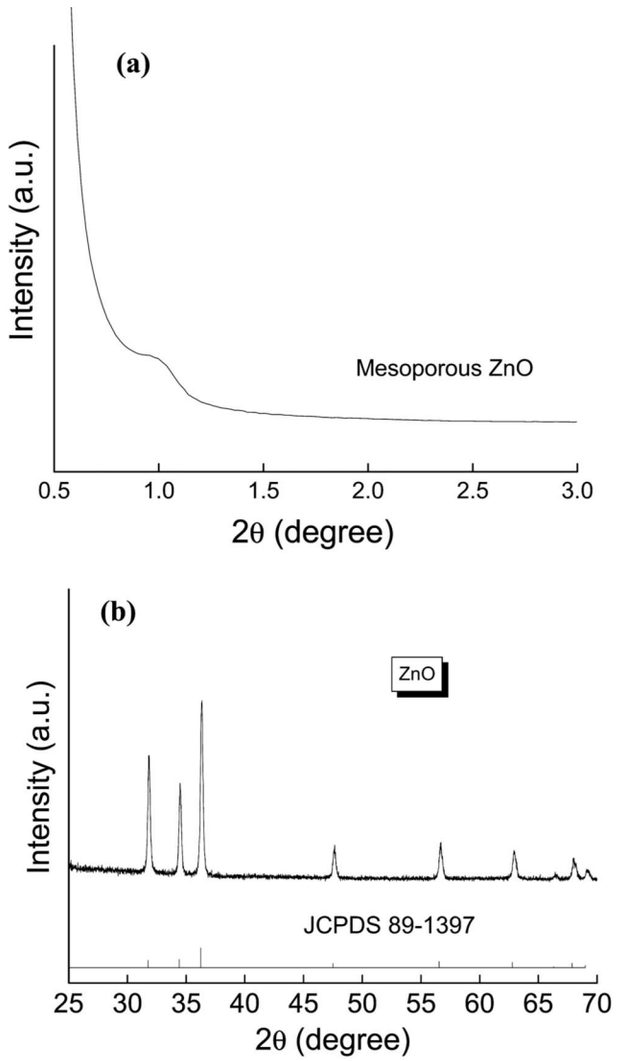

Figure 1. (a) Low-angle XRD patterns and (b) wide-angle XRD patterns of the mesostructured ZnO.

using a JEOL-2100F electron microscope at 200 kV. Sine-wave signals of 1 MHz and 10 V amplitude (peak-to-peak) were chosen to enable the mesoporous carbons to be deposited onto the electrode gap using DEP forces. The gas-sensing properties were characterized using a computer-controlled gas-sensing characterization system. The test gas was 10–100 ppm CO in dry air, injected into the chamber at a total flow rate of 100 sccm. After some time, the chamber was purged with air and the experiment was repeated. The electrical resistance response during testing was monitored using a precision analyzer (Keithley 2400). The sensor response (S) was defined as follows: $S = (R_{CO} - R_{air}/R_{air})^* 100\%$, where R_{air} and R_{CO} represent the resistance of the sensor in air and in CO gas, respectively. The response time to CO gas was defined as the time required for 90% of total resistance to the gas.

Results and Discussion

The low-angle XRD pattern of porous ZnO is shown in Fig. 1a, which gives the structural order of the mesoporous ZnO. The figure indicates that the sample has a clearly defined diffraction peak located at approximately at 1.0° which can be attributed to the (100) reflections of the hexagonal groups. It also indicates that the sample exhibits a well-ordered structure. Moreover, the cell parameter of

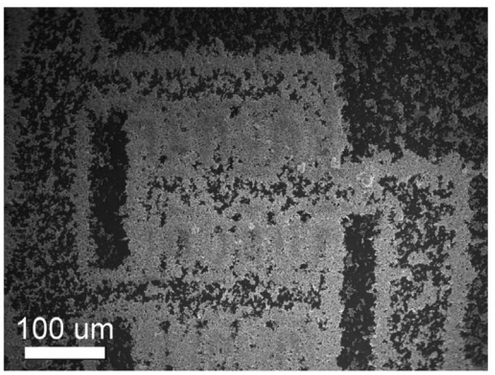

Figure 2. SEM image of DEP immobilized mesostructured ZnO.

mesostructured ZnO is 10.35 nm. The peaks in the wide-angle region (Fig. 1b) are located at 30.9, 33.4, 35.2, 46.0, 54.5, 60.5, 65.3, and 66.4° and correspond to a crystalline ZnO structure. These patterns also indicate the mesostructured ZnO has a *c*-axis preferred orientation. This is consistent with conventional bulk ZnO samples. The morphology of the mesostructured ZnO is confirmed by SEM in Fig. 2. The image indicates the mesostructured ZnO particles seem to be randomly oriented. The randomly oriented particles provide electrical paths between neighboring extrusions. When these randomly oriented mesostructured ZnO are in the spacer regions, the two electrodes are no longer electrically open. The ordered structure and the crystallization of porous ZnO were determined by TEM and SAED, as shown in Fig. 3. The TEM image shows the hexagonal arranged well-ordered structure; the SAED pattern also shows the diffraction rings, implying that the mesostructured ZnO is polycrystalline. However, during the calcination process, the ZnO particles are aggregated and overlapped. Therefore, larger nanograins are observed. In order to investigate this phenomenon, a dark-field TEM image is examined. One particle with a nanograin having a size of approximately 20 nm is observed (Fig. 3c). Therefore, the sizes of the nanograins of mesostructured ZnO are approximately 20 nm. The high-resolution-TEM image also indicated that the *d*-spacing of porous ZnO was 0.24 nm, which is consistent with the XRD results. The surface area and pore volume of mesostructured ZnO are 61.3 $m^2\ g^{-1}$ and 0.31 $cm^3\ g^{-1}$, respectively. The pore diameter distribution determined by the BJH method showed a pronounced peak at 5.7 nm (not shown here), confirming a high degree of uniformity among the pores. The adsorption of oxygen forms ionic species such as O^{2-}, O_2^-, and O^-, which are adsorbed onto the mesostructured ZnO surface at elevated temperatures. The form of the oxygen ionic species is strongly dependent upon the temperature. In general, O_2^- is predominant at temperatures below 100°C, O^- between 100 and 300°C, and O^{2-} above 300°C.[19] The resistance of the mesostructured ZnO sensor decreases upon the introduction of CO gas because of the exchange of electrons between the ionosorbed oxygen and the mesostructured ZnO sensor.[20] For semiconductor gas sensors, it is known that oxygen sorption plays an important role in electron transport. The oxygen sorption affects the conductivity of ZnO.[21] Therefore, the sensing mechanism of the nanostructured ZnO sensor for CO may be described through reaction kinematics in the following equations[22]

$$O_{2(gas)} \leftrightarrows O_{2(absorbed)} \quad [1]$$

$$O_{2(absorbed)} + e^- \leftrightarrows O_2^- \quad [2]$$

$$O_2^- + e^- \leftrightarrows 2O^- \quad [3]$$

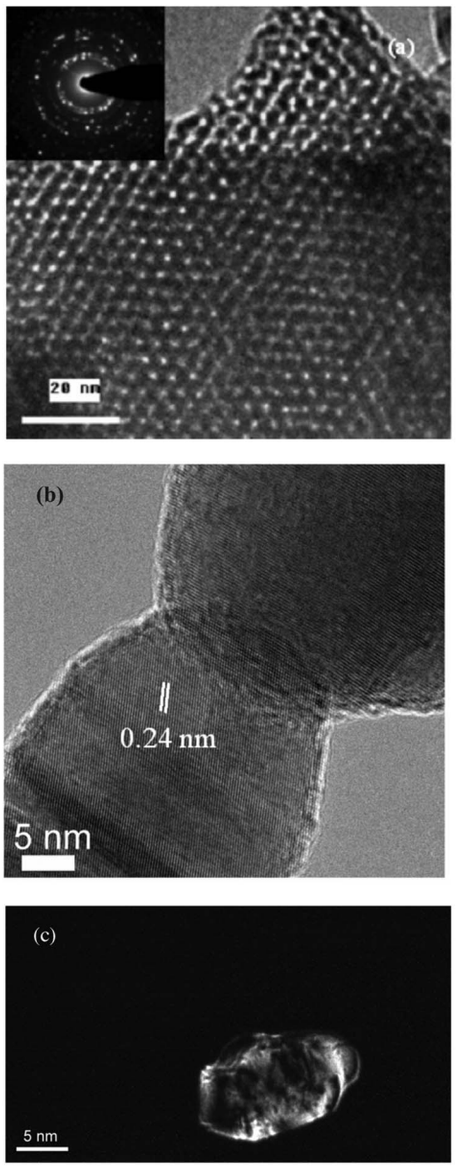

Figure 3. (a) TEM image of mesostructured ZnO materials as a replica of a mesoporous carbon template. (b) High-resolution TEM micrograph of the crystalline framework of mesostructured ZnO. (c) Dark-field TEM image of mesostructured ZnO materials.

The reaction between CO gas and the ZnO surface, however, can be shown as follows[23]

$$2CO + O_2^- \rightarrow 2CO_2 + e^- \quad [4]$$

$$CO + O^- \rightarrow CO_2 + e^- \quad [5]$$

$$CO + O^{2-} \rightarrow CO_2 + 2e^- \quad [6]$$

Figure 4 shows the effect of the working temperature on the sensitivity of the porous ZnO sensor toward CO. It shows that the working temperature plays an important role in the sensitivity of the porous ZnO sensor. At a low operation temperature, a low sensitivity can be expected because the CO molecules do not possess sufficient thermal energy to react with the surface adsorbed oxygen species, O_2^-, i.e., the reaction rate given by Eq. 4 is essentially low. However, as the temperature was increased to 250°C, the adsorbed oxygen

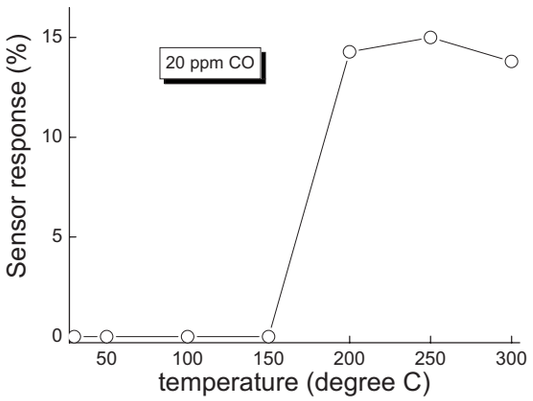

Figure 4. Variation of sensing response of mesostructured ZnO sensor with temperature at 20 ppm CO.

was converted from O_2^- to O^-, and the CO sensing reaction was then given by Eq. 5. The increase in sensitivity for temperatures above 300°C can be attributed to the fact that the thermal energy obtained was sufficiently high to overcome the activation energy barrier to the reaction and the electron concentration increased significantly due to the sensing reaction, as indicated by Eq. 3, in which a maximum sensitivity of 15.0% was found for the mesostructured ZnO sensor. The reduction in sensitivity above a temperature of 250°C was due to the difficulty in exothermic CO gas adsorption; therefore, an optimum operating temperature should be considered in order to obtain a high sensitivity. Similar temperature dependence has also been observed.[24] The sensor response increases to the maximum at 250°C, which is the threshold temperature for sensing CO gas. Wang et al. have indicated that ZnO-nanorod-based CO gas sensors can be used to perform measurements at 250°C. The sensor response was very low for ZnO nanorods to CO gas.[25] Hsueh et al. have shown that the optimum sensor response of the ZnO-nanowire-based CO sensor for 500 ppm CO gas was 57%.[26] However, no response was detected at lower CO concentrations. Figure 5 shows the variation in sensitivity of the ZnO sensor in relation to its exposure to CO gas injection. It was found that the optimum sensitivities of the ZnO sensor are 12.1, 14.6, 18.4, 26.0, and 60% at CO concentrations of 10, 20, 30, 50, and 70 ppm, respectively. This shows that the porous ZnO gas sensor has a high response at low CO concentrations. Recently, Malagù et al. demonstrated an enhancement in sensitivity when the grain size of the semiconductive oxide is below 10 nm.[27] They described a model where the surface acceptor density decreases when the mean grain size is increased for

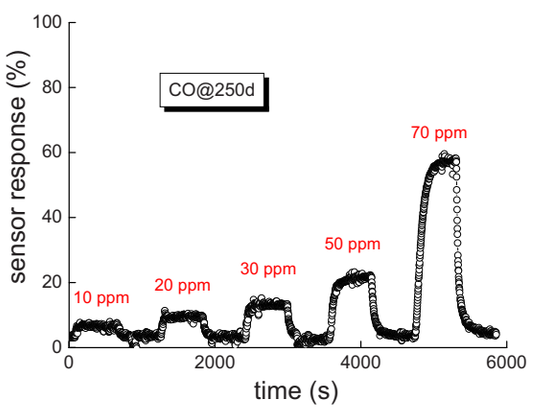

Figure 5. (Color online) Sensing response of mesostructured ZnO sensor determined with several CO concentrations.

n-type semiconductive oxides. The CO response can be enhanced through a reduction in the surface charge accumulation, induced through a decrease in grain size. Williams and Coles agreed with this model.[28] The presence of the uniform mesopores in a porous ZnO sensor can also be another important reason for the high response for CO gas. The pores in the ZnO sensor can enhance the detection of gas molecules passing through and create more active sites to adsorb oxygen ions. As shown in Fig. 5, the response and recovery times of the nanostructured ZnO sensor were found to be 80 and 90 s, respectively. The response and recovery times are shorter than when other materials are used, especially the recovery time. These results indicate that the response speed and the stability of the porous ZnO sensor are both good.

Conclusion

This study presented the porous metal oxide ZnO, synthesized through a template replication method. Mesoporous carbon was successfully used as a hard template for synthesizing porous ZnO. The structural property of the porous ZnO was polycrystalline and exhibited a highly ordered structure. The surface area, pore volume, and pore size of the porous ZnO were 61.3 $m^2\ g^{-1}$, 0.31 $cm^3\ g^{-1}$, and 5.3 nm, respectively. The development of highly ordered porous ZnO and the fabrication of a nanostructured porous ZnO-based CO sensor were also reported. This device has high sensitivity to CO ($\sim$60%) at 250°C and both the response and recovery times were fast (80 and 90 s). Furthermore, the response speed and stability of this device were demonstrated to be good as well.

Acknowledgments

The authors thank the National Science Council of the Republic of China, Taiwan, for financially supporting this research under contract no. NSC 96-2221-E-451-013. The authors are also grateful to the Center for Nanoscience and Technology of the National Chiao-Tung University for its assistance with the TEM and XRD characterizations.

National Chiao-Tung University assisted in meeting the publication costs of this article.

References

1. G. Neri, A. Bonavita, S. Galvagno, P. Siciliano, and S. Capone, *Sens. Actuators B*, **82**, 40 (2002).
2. M. C. Horrillo, A. Serventi, D. Rickerby, and J. Gutierrez, *Sens. Actuators B*, **24/25**, 465 (1995).
3. N. Kumar, A. Dorfman, and J. Hahm, *J. Nanosci. Nanotechnol.*, **5**, 1915 (2005).
4. N. Koshizaki and T. Oyama, *Sens. Actuators B*, **66**, 119 (2000).
5. J. N. Zeng, J. K. Low, Z. M. Ren, T. Liew, and Y. F. Lu, *Appl. Surf. Sci.*, **197**, 362 (2002).
6. J. H. Lee, K. H. Ko, and B. O. Park, *J. Cryst. Growth*, **247**, 119 (2003).
7. T. Wagner, C. D. Kohl, M. Fröba, and M. Tiemann, *Sensors*, **6**, 318 (2006).
8. H. Yang, Q. Shi, B. Tian, Q. Lu, F. Gao, S. Xie, J. Fan, C. Yu, B. Tu, and D. Zhao, *J. Am. Chem. Soc.*, **125**, 4727 (2003).
9. J. H. Smått, B. Spliethoff, J. B. Rosenholm, and M. Lindén, *Chem. Commun. (Cambridge)*, **2004**, 2188.
10. C. Dickinson, W. Chou, R. P. Hodgkins, Y. Shi, D. Zhao, and H. He, *Chem. Mater.*, **18**, 3088 (2006).
11. B. Tian, X. Liu, H. Yang, S. Xie, C. Yu, and D. Zhao, *Adv. Mater. (Weinheim, Ger.)*, **15**, 1370 (2003).
12. B. Tian, X. Liu, L. A. Solovyov, Z. Liu, H. Yang, Z. Zhang, S. Xie, F. Zhang, B. Tu, C. Yu, et al., *J. Am. Chem. Soc.*, **126**, 865 (2004).
13. M. Kang, S. H. Yi, H. I. Lee, J. E. Yie, and J. M. Kim, *Chem. Commun. (Cambridge)*, **2002**, 1944.
14. J. Roggenbuck, H. Schäfer, T. Tsoncheva, C. Minchev, J. Hanss, and M. Tiemann, *Microporous Mesoporous Mater.*, **101**, 335 (2007).
15. A. Dong, N. Ren, Y. Tang, Y. Wang, Y. Zhang, W. Hua, and Z. Gao, *J. Am. Chem. Soc.*, **125**, 4976 (2003).
16. W. J. Moon, J. H. Yu, and G. M. Choi, *Sens. Actuators B*, **87**, 464 (2002).
17. C. Y. Liu, C. F. Chen, J. P. Leu, and Y. C. Lin, *J. Sol-Gel Sci. Technol.*, **43**, 47 (2007).
18. K. Böhme, W. D. Einicke, and O. Klepel, *Carbon*, **43**, 1918 (2005).
19. M. Takata, D. Tsubone, and H. Yanagida, *J. Am. Ceram. Soc.*, **59**, 4 (1976).
20. B. L. Zhu, D. W. Zeng, J. Wu, W. L. Song, and C. S. Xie, *J. Mater. Sci.*, **14**, 521 (2003).
21. P. Mitra, A. P. Chatterjee, and H. S. Maiti, *Mater. Lett.*, **35**, 33 (1998).
22. P. P. Sahay, *J. Mater. Sci.*, **14**, 4383 (2005).
23. S. R. Morrison, *Sens. Actuators B*, **84**, 258 (2002).
24. J. F. Chang, H. H. Kuo, I. C. Leu, and M. H. Hon, *Sens. Actuators B*, **84**, 258 (2002).
25. J. X. Wang, X. W. Sun, Y. Yang, H. Huang, Y. C. Lee, O. K. Tan, and L. Vayssieres, *Nanotechnology*, **17**, 4995 (2006).
26. T. J. Hsueh, Y. W. Chen, S. J. Chang, S. F. Wang, C. L. Hsu, Y. R. Lin, T. S. Lin, and I. C. Chen, *Sens. Actuators B*, **125**, 498 (2007).
27. C. Malagù, V. Guidi, M. Stefancich, M. C. Carotta, and G. Martinelli, *J. Appl. Phys.*, **91**, 808 (2002).
28. G. Williams and G. S. V. Coles, *MRS Bull.*, **24**, 25 (1999).